01 Jan 2023

Densifying Hydration Products of Alite by a Bio-Inspired Admixture

Yi Fang

Jialai Wang

Liang Wang

Xin Qian

et. al. For a complete list of authors, see https://scholarsmine.mst.edu/civarc_enveng_facwork/2263

Recommended Citation

Y. Fang et al., "Densifying Hydration Products of Alite by a Bio-Inspired Admixture," *Materials and Design*, vol. 225, article no. 111490, Elsevier, Jan 2023.
The definitive version is available at https://doi.org/10.1016/j.matdes.2022.111490

Materials & Design 225 (2023) 111490

Contents lists available at ScienceDirect

Materials & Design

journal homepage: www.elsevier.com/locate/matdes

Densifying hydration products of alite by a bio-inspired admixture

Yi Fang [a,b], Jialai Wang [b,*], Liang Wang [c], Xin Qian [d,*], Xiaodong Wang [b], Wenyu Liao [e], Peiyuan Chen [c], Hongyan Ma [e]

[a] College of Mechanics and Materials, Hohai University, Nanjing, Jiangsu 211100, PR China
[b] Department of Civil, Construction, and Environmental Engineering, The University of Alabama, Tuscaloosa, AL 35487, United States
[c] School of Civil Engineering and Architecture, Anhui University of Science and Technology, Huainan 232001, Anhui, PR China
[d] Key Laboratory of Infrastructure Durability and Operation Safety in Airfield of CAAC, Tongji University, Shanghai 201804, PR China
[e] Department of Civil, Architectural and Environmental Engineering, Missouri University of Science and Technology, Rolla, MO 65401, United States

HIGHLIGHTS

- Tannic acid (TA) can be used to mediate the hydration of tricalcium silicate (alite) to achieve better microstructure.
- TA can form complex with calcium ion through chelating, thus retarding the hydration of the alite.
- TA can promote the growth of calcium hydroxide along x-axis.
- TA can modify the atomic structure of calcium silicate hydrate.
- TA has a unique ability to radically reduce inter-hydrate pores of cement paste.

GRAPHICAL ABSTRACT

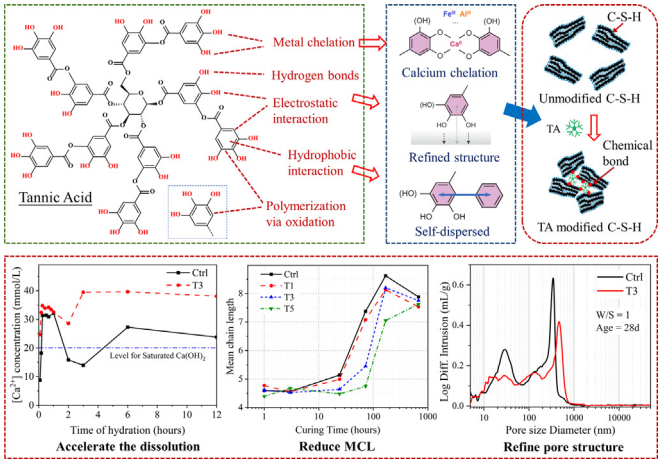

ARTICLE INFO

Article history:
Received 27 April 2022
Revised 7 December 2022
Accepted 10 December 2022
Available online 10 December 2022

Keywords:
Tricalcium silicate
Tannic acid
Bioinspiration
Admixture
C—S—H

ABSTRACT

A bio-inspired, plant-derived polyphenol, tannic acid (TA) was identified as a renewable admixture to improve the compressive strength of concretes. Aiming to understand the underlying mechanism responsible for this strength improvement, this study examines how TA mediates the hydration of tricalcium silicate (alite). Experimental study shows that TA can form complex with calcium ions through chelating, retarding the hydration of the alite and changing of the hydration products. Particularly, X-ray diffraction analysis shows that TA makes calcium hydroxide preferentially grow on the [001] face. Fourier-transform infrared spectroscopy and ^{29}Si MAS NMR results reveal that the mean chain length of calcium silicate hydrate (C—S—H) is reduced by TA. More importantly, mercury intrusion porosimetry testing reveals that pores with size near 30 nm was almost eliminated by adding TA, leading to higher elastic modulus of the produced C—S—H and higher compressive strength of the produced concrete.

1. Introduction

Concrete with ordinary Portland cement (OPC) as the binder is the most widely used infrastructure material, and its production

* Corresponding authors.
E-mail addresses: jwang@eng.ua.edu (J. Wang), xqian2@tongji.edu.cn (X. Qian).

https://doi.org/10.1016/j.matdes.2022.111490
0264-1275/

is expected to increase at a rate of 5% annually [1]. The manufacturing of cement produces a large amount of greenhouse gases [1,2]. In general, the production of one ton of OPC emits 0.912 tons of CO_2 [3]. An effective approach to decarbonize OPC based concretes is to enhance their strength and durability so that less cement and concrete are needed. To achieve "significant" improvement, the desirable admixture may need to prominently modify the nano- and micro-structures of the major hydration product of OPC (i.e., C—S—H). Extensive studies on C—S—H phase [4–7] indicate that the mechanical performance of concrete may be enhanced by improving the "intrinsic" cohesion of C—S—H phase itself, which is more fundamental and probably more effective than traditional methods (i.e., improving degree of hydration and packing). Pellenq et al. [5] have proposed two possible strategies to modify the bonding scheme of C—S—H phase at molecular scale. One (named herein the "inorganic approach") is to enhance cohesion by either increasing the ionic-covalent and ion correlation bonds or modifying the microstructure to optimize connectivity of C—S—H nanoparticles; and the other (named herein "organic–inorganic hybridization") is to graft small organic groups or polymeric chains into growing C—S—H phase to achieve covalent hybridization, to improve the fracture energy and strain capacity. Attempts following the former strategy have been limited, and recent studies have shown that stoichiometric modifications of C—S—H (e.g., changing the Ca/Si ratio and replacing Si by Al and Fe) might be inefficient in significantly improving the mechanical and physical properties of the gel [8–10].

Much more efforts have been made on exploring the feasibility of organic–inorganic hybridization. Organic matters that have been used include poly(methacrylic acid), poly(acrylic acid), Poly(vinyl sulfonic acid), poly(vinyl alcohol) (PVA), poly(ethylene glycol), Poly(allylamine), polysacchrides, celluloses, and so on [11–14]. These polymers were selected because their molecular structures contain plenty of functional groups [e.g., anionic: carboxyl and sulfonate; or nonionic: hydroxyl, alkoxy, carbonyl, and amino] which can interact with C—S—H. It has been agreed that functional groups with higher polarity presents better affinity to C—S—H (e.g., —OH, —COO—, and =O > NH_2) [15]. The functional groups not only improve H-bonds (both number and strength) and electrostatic forces at C—S—H/polymer interfaces, but also fill into the defects/damages of the silicate chains, repairing defective silicate chains that are supposed to be broken during fracture process (e.g., by forming Si—O—C bonds) [12]. However, most of these efforts failed to improve the bulk mechanical properties such as indentation modulus, hardness, and strength of the C—S—H/polymer composite (though creep modulus is often improved) [12], which could be attributed to the steric, entropic, or electrostatic interactions which tend to hinder the entry of organic molecules (especially ones with large molecular weights) into C—S—H [16]. To overcome such hindrance, some researchers have tried to design short-chained or small organic molecules containing highly polarized and/or reactive functional groups, such as short-chained PVA [12]. These efforts did achieve some improvement in mechanical performance for the produced C—S—H/polymer nanocomposites.

So far, all relevant studies on organic–inorganic hybridization have been limited to synthetic C—S—H/polymer composites and/or MD simulations. Success has not yet been achieved on any practical OPC-based systems. Recognizing the limitations of traditional monomers and polymers used in existing studies, we turn to nature for a solution since nature may have created the best organic molecules, which are naturally abundant (thus eco-friendly and economical), of appropriate size, and containing highly effective functional groups for concrete. This is echoed by a recent overview [1], which suggests that "bio-based molecules greatly broaden the range of possibilities regarding molecular and polymer complexity and offer higher specificity for interaction with targeted cement phases."

Bioinspired arena provides a useful hint to identify such bio-based molecules. Mussels can attach to various underwater substrates, ranging from inorganic materials and organic natural materials to synthetic materials, using adhesive proteins [17,18] L-3,4-dihydroxyphenylalanine (DOPA) in the mussel byssus. With a catechol-type functionality (i.e., an aromatic ring with two hydroxyls on neighbouring carbons), DOPA can complex or cross-link macromolecules sites through multiple interactions interact with $\pi - \pi$ stacking, covalent doping, protein – protein binding, metal chelation [19] and hydrogen bonding [19]. Inspired by the outstanding adhesion brought about by catecholic compounds, extensive studies have been carried out to exploit catechols as binding agent in synthetic materials [20]. It is not easy to directly use DOPA as a binding agent. Therefore, Dopamine, a chemical analogue of DOPA, is commonly in existing studies. For example, Zohhadi found that the compressive and splitting tensile strength of the cement mortar were improved by on average by 55% and 27%, respectively, after dopamine at a 0.5 wt% of cement was added [21]. Fang et al shows that coating very fine sand with a layer of polydopamine can significantly enhance the strength of the produced cement mortar [22]. Using a thermodynamic binding model, Jenness and Shukla show dopamine-doping can increase the strength of concretes through binding to various oxides found in concrete mixtures [23].

However, the high cost of dopamine prohibits its practical application in concretes. Therefore, a low-cost alternative, tannic acid (TA) has been extensively used in the literature [24–27]. TA is the third widely available bio-based molecules, only after cellulose and lignin [28]. Similar to dopamine, TA is a catecholic compound with a claw-shaped structure and higher density of functional groups (i.e., hydroxyl and ester bonds), as shown in Fig. 1. With abundant reactive terminal phenolic hydroxyl groups, TA has a similar ability as DOPA and dopamine, as shown in Fig. 1 [24–27,29,30]. Tannic acid is soluble in water and can be hydrolyzed in acidic or alkaline surroundings, resulting glucose and phenolic acids such as gallic acid [31]. The covalent bonds between tannic acid during the polymerization process, which is the oxidization of polyphenols to quinones and their subsequent condensation, can help to improve the strength of structure [32,33]. In alkaline condition, the hydrolysis of TA allows an increase in the charge density of tannin via ionization of phenolic hydroxyl groups and dissociation of ester bonds and phenolic groups, leading to increase of steric forces including steric hindrance and electrostatic repulsion force [34]. This indicated that TA has the ability to disperse grain particles in high pH condition, which matches up the demand of cementitious materials. Therefore, TA can be used to as a new admixture to enhance the performance of concretes, which has been confirmed by our previous studies [35–38].

Aiming to understand the mechanisms responsible for the enhanced performance of the concrete induced by doping TA, this study examined how TA affect the hydration of the cement and major hydration products, especially C—S—H. To this end, tricalcium silicate (C_3S), known as alite for its impure form, was used to exclude the influence from other phases. The hydration kinetics of the alite were first studied by isothermal micro-calorimetry. Kinetic parameters were obtained based on the calorimetry data using boundary nucleation and growth model (BNG). X-ray diffraction (XRD) and thermogravimetric analysis (TGA) were used to examine the hydration products. Fourier-transform infrared spectroscopy (FTIR) and ^{29}Si MAS NMR were used to detect chemical interaction between TA and C—S—H. The pore structure of the produced TA modified alite pastes was examined by mercury intrusion porosimetry (MIP). Micromechanical properties of the produced TA modified hydration products were examined by nanoindentation.

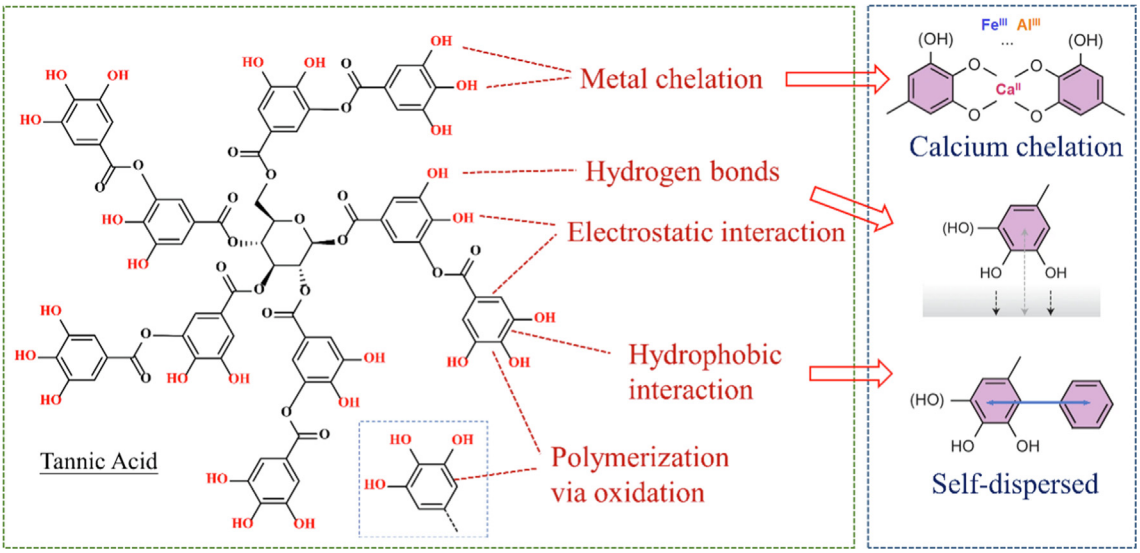

Fig. 1. Molecular structure of TA and its multiple interaction concluding covalent and non-covalent interactions.

2. Materials and methods

2.1. Materials

Alite (C_3S) powder was purchased from Kunshan Overseas Chinese Technology New Materials Co., ltd. The composition and physical characteristics of the alite is presented in Table 1. The crystalline compositions of the raw material were characterized by XRD (Rigaku Smartlab, Japan, Copper K-α) as shown in Fig. S1 (see supplementary material). The C_3S purity was 93.4 wt% obtained by the Rietveld refinement method. The impurities were β-C_2S. TA ($C_{76}H_{52}O_{46}$, 98%) was purchased from Alfa Aesar. TA solution was obtained by agitating TA powder in deionized water for 2 mins. Deionized water or TA solution was mixed with the alite powder to make alite pastes at a water-to-binder ratio (*w/b*) of 1.0. To evaluate the atomic absorption of calcium ions and pH value of the pore solution, the *w/b* of the alite slurry was used as 2.0 to prevent the congealing and hardening of the pastes. The control group (Ctrl) was made with only alite and water; and three TA-incorporated pastes, T1, T3, and T5 were made by adding 0.1%, 0.3%, and 0.5% TA by weight of alite to the control paste, respectively.

2.2. Micro-calorimetry test

The kinetics of the hydration of C_3S was monitored by a TAM IV isothermal conduction micro-calorimeter, programmed to maintain the sample at a constant temperature of 20 ± 0.1 °C. Compared to conventional reactivity assessment methods (e.g., isothermal calorimetry), the micro-calorimetry method is deemed more accurate as it allows quantification of the reaction's heat flow rate at a very high resolution (10^{-7} J/s). To do this, specific amount of alite was first measured and placed in the ampule. Then deionized water or TA solution was introduced with *w/b* of 1.0 and mixed at a constant speed for 1 min in the ampule. After that, the ampule was sealed with a cap and placed into the testing chamber of the calorimeter. The time from contacting with water to introducing the mixture into the calorimeter was limited to be 4 ± 1 min. The system was equilibrated for 15 min before starting to record the heat release from the mixture.

2.3. Boundary nucleation and growth model

A kinetic model based on the formation of C—S—H was introduced to evaluate the effect of TA on the hydration of alite. In boundary nucleation and growth models (BNG), C—S—H is usually nucleated and grown at a specific site near the boundary of the untransformed state by heterogeneous nucleation rather than homogeneous nucleation between the reacting domains [39,40]. Thomas's BNG model [41,42] was adopted in this work to allow for growth of C—S—H from a constant number of nuclei or with a constant nucleation rate. In this model, the volume fraction of the hydration products at any given time t based on constant nucleation rate is given by

$$X = 1 - \exp\{-2O_v G(t-t_0)\int_0^1 [1-\exp(-\frac{\pi}{3} I_B G^2 (t-t_0)^3 (1-u^2) \times (1+u))]du\} \quad (1)$$

where G is the growth rate, I_B is the nucleation rate (per unit area of substrate per unit time), t_0 is the time delay when the particular region nucleated (or induction time), and O_v is the amount of substrate per unit volume in the system, related to the surface area of alite particles by the following relation [42]

$$O_v = \frac{S_{BET}}{R_{wc}/\rho_w + 1/\rho_c} \quad (2)$$

where R_{wc} is the mass ratio between water and alite, ρ_w is the density of water, and ρ_c is the density of alite, which is assumed as 3.12×10^3 kg/m^3 [43].

Table 1
Chemical composition and BET area of analytical alite powder.

BET area (m^2/g)	D_{50} particle sizes (μm)	Chemical composition / %					
		CaO	SiO_2	SO_3	Fe_2O_3	Al_2O_3	MgO
1.978	3.5	83.9	16.1	0	0	0	0

If the number of nuclei per unit area of the grain has the constant value *Ns*, the kinetic equation (1) is replaced by:

$$X = 1 - \exp\{-2O_v G(t - t_0) \int_0^1 [1 - \exp(-\pi NsG^2(t - t_0)^2(1 - u^2))]du\} \quad (3)$$

To apply the BNG model to the calorimetry data, the rate of heat evolution is defined as

$$Rate = AdX/dt \quad (4)$$

where *A* is a scaling parameter related to the activation energy.

The integration and differentiation were carried out numerically using a simple MATLAB program. The model was fitted manually to achieve a good agreement between the kinetic data and the BNG model in the region of the main rate peak.

2.4. Atomic absorption spectroscopy and pH value of the pore solution

The pore solutions of the hydrated alite were prepared to study the adsorption property of TA. To this end, a control alite slurry (Ctrl) was prepared by adding 2 g alite powder in 4 g DI water under continuously stirring. The TA doped alite slurry (T3) was produced by mixing 2 g alite powder with a TA solution prepared by dissolving 0.006 g TA powder into 4 g DI water. The produced alite slurries were sampled at the following ages: 5 min, 10 min, 15 min, 20 min, 25 min, 30 min, 40 min, 50 min, 60 min, 2 h, 3 h, 6 h, and 12 h. The pore solutions were obtained by centrifuging the slurries with high speed and then filtering via vacuum. To meet the requirement on the test range of ion concentration, these pore solutions were diluted 50 times with DI water before testing [44].

The total amount of calcium in the pore solution was measured by a TAS-986 atomic absorption spectroscope (AAS). The wavelength of the calcium element was chosen as 422.7 nm for higher sensitivity. The currents of the instrument and preheat lamp were 3 mA and 2 mA, respectively. The passband width for the spectrum was 0.4 nm. The flow rate of gas was 1700 mL/min and the height of the burner was 6 mm. Before the measurement, the instrument was calibrated by a standard solution containing specified amount of calcium element. Besides, the alkali level of the solution was monitored by a Mettler Toledo pH meter.

2.5. Characterization of hydration products

For the control and TA-modified pastes, six curing ages (i.e., 1 h, 3 h, 24 h, 3d, 7d, and 28d) were used to test the influence of TA on the hydration products of C_3S and paste microstructure. For each group and each curing ages, 1 g deionized water or TA solution was mixed with 1 g alite powder to make alite pastes in the hexagonal weighting dishes. All the samples were cured in sealed condition with Parafilm laboratory film at room temperature. Hydration was arrested at the specified age by sub-merging the samples in isopropanol for 24 h. These samples were then dried in a vacuum desiccator for more than 24 h at room temperature. The samples were downsized/fractured for MIP analyses, and were pulverized into fine powder (passing through #200 sieves) using an agate mortar and pestle for XRD, TGA, and FTIR analyses. Before the tests, the sample was stored in a closed vessel under a light vacuum.

2.5.1. XRD

The XRD analysis was carried out by using a Bruker D8 Discover with GADDS with the scan range 15–70°. Two separate frames were integrated for the final pattern. Each frame period runs 180 s with Co (40 kV, 35 mA) source and scan step 0.005°/s.

2.5.2. TGA

TGA analysis was carried out using a PerkinElmer STA 8000 instrument. For each test, the sample was first held at 30°C for 30 min and then heated from 30 °C to 950°C at 10.00 °C /min under N_2 purge at a flow rate of 100 mL/min.

The hydration of alite is followed by the precipitation of nanocrystalline C—S—H phase and the crystallization of CH, see overall reaction (5) [45]:

$$Ca_3SiO_5 + 5.2\ H_2O \rightarrow 1.2Ca(OH)_2 + (CaO)_{1.8}SiO_2(H_2O)_{4.0} \quad (5)$$

According to the DTG results, C—S—H phases start to lose weight from 30°C to 550°C due to the dehydroxylation or loss of interlayer water [46]. The mass loss between 30°C and 550°C was regarded as the amount of bound water, as given by equation (6). The weight loss related to the decomposition of CH can be measured by integrating the peak area between 400°C and 525°C in DTG curves [47]. This tangential method can correct the overestimation of CH and exclude the weight loss caused by the ongoing decomposition of C—S—H in this temperature interval [46]. The weight loss related to C—S—H can be obtained by subtracting the part of CH from the total bound water. Then the amount of CH can be calculated via using the molecular masses of portlandite (74 g/mol) and water (18 g/mol) (equation (7)). The amount of C—S—H is measured based on the assumption of losing all the water in the C—S—H according to equation (8). The quantifications of CH, C—S—H, and bound water are normalized to the dry binder weight at 550°C [48], as given by equation (6–8):

$$W_{[H_2O]} = \frac{M_{30} - M_{550}}{M_{550}} \times 100(\%) \quad (6)$$

$$W_{[Ca(OH)_2]} = \frac{(M_{400} - M_{525})_{tangential}}{M_{550}} \times \frac{74}{18} \times 100(\%) \quad (7)$$

$$W_{[C-S-H]} = \frac{(M_{30} - M_{500}) - (M_{400} - M_{525})_{tangential}}{M_{550}} \times \frac{232.8}{72} \times 100(\%) \quad (8)$$

2.5.3. FTIR

The characteristic stretching vibrations of Si-O bonds in C—S—H can be detected by FTIR. The presence and intensity of the end silicate tetrahedra (Q^1) and bridging silicate tetrahedra (Q^2) can be detected by the FTIR spectra according to the reference [49]. The FTIR spectra were acquired by a PerkinElmer Spectrum 2 with an attenuated total reflectance (ATR) accessory. The wavenumbers of the IR spectra were collected from 650 cm^{-1} to 4000 cm^{-1}. Only the interval between 650 cm^{-1} and 2000 cm^{-1} is reported in the related graphs for this paper. The mean chain length (MCL), which measures the polymerization of silicate chains in C—S—H [50,51], is computed based on the peak intensity ratio of the Q^1 signal at ~ 810 cm^{-1} and the main peak at ~ 960 cm^{-1} and using the ratio of $2(Q^1 + Q^2)/Q^1$ according to the reference [52].

2.5.4. ^{29}Si MAS NMR

^{29}Si MAS NMR can also provide quantitative analysis of the silicate chain atomic structure of C—S—H and was used to compare with the similar information collected from FTIR. Bruker Avance 400 NMR spectrometer was utilized to collect the spectra with a 7 mm CP/MAS probe. Tetramethylsilane (TMS) was used as an external standard at 0 ppm to measure the chemical shifts. The measurements were performed using 1024 scans, a dwell time of 15.7 s, and a 6 s pre-scan delay. The spectral deconvolution was performed with MestReNova with a Lorentzian/Gaussian ratio of 0.5.

2.5.5. MIP

Effect of TA on the pore structure of the alite pastes was evaluated by MIP with a Micromeritics AutoPore IV 9500. The samples

were obtained by cutting the cubic alite pastes after 28d of moist curing. Tips given in [53] were followed to characterize the pore structure.

2.5.6. Nanoindentation

Nanoindentation testing was carried out to reveal the micromechanical properties of the hardened alite paste. The pastes with a w/s ratio of 1.0 was moist cured in a cubic mould with a size of 20 mm × 20 mm × 20 mm at room temperature for 28 days. The cement paste pieces were cast into a capsule filled with epoxy resin, followed by polishing successively with SiC sanding paper and diamond suspension on felt cloths. The final two polishing steps used 0.3 μm and 0.05 μm alumina suspensions, respectively. A Hysitron TI950 nanoindenter with a Berkovich diamond tip was used to make 400 indents in a 20 × 20 grid with a 10 μm spacing. The indentation load was increased by multiple partial unloading (10 times) with the maximum load 1 mN, as mentioned in previous work [36]. Multiple cycles of partial loading and unloading were chosen to make each indent, thereby eliminating the creep, surface roughness and size effects [54]. The elastic modulus was calculated by using the Oliver and Pharr method [55].

For quantitative analysis of grid indentation, it is essential to apply statistical deconvolution techniques to determine the volume fractions and the average mechanical properties. The deconvolution process was performed on MATLAB by using Gauss Mixture Model (GMM). The indents on C—S—H phases were recognized by the elastic modulus smaller than the C—S—H particle stiffness ($E \leq 60$ GPa) [56]. Three phases of hydration products (excluding anhydrous clinker minerals) can be identified based on the deconvolution results, which are low-density C—S—H (LD), high-density C—S—H (HD), and ultra-high density C—S—H which essentially is a mix of C—S—H and portlandite (UHD) [57,58].

3. Experimental results

3.1. Micro-calorimetry test and BNG simulation

Fig. 2 compares the hydration kinetics of C_3S without (Ctrl) and with TA (T1, T3, and T5) up to 150 h. The rate of heat evolution of the hydration of C_3S without TA exhibits typical features of the hydration of OPC, consisting of four periods: the initial period, the induction period, the acceleratory period, and the deceleration period. A rapid heat evolution occurs at the very beginning of the testing curve (initial period) due to wetting of C_3S and dissolution of different ions. After this initial period, the rate of heat evolution drops with time and the hydration of the cement enters the induction period. The acceleratory period started at 2 h in which the hydration accelerated with time and the peak rate of heat evolution occurred at ≈ 12 h of hydration, followed by the deceleration period.

By adding 0.1% TA to the paste, the hydration kinetics was drastically changed, as shown in Fig. 2. First, the induction period is extended from 2 h to 10.5 h. Second, the peak of the thermal power in the acceleratory period is not only delayed from 11.6 h to 27.6 h, but also reduced to 65% of that of the control sample. These two features clearly indicate the strong retarding effect of TA. However, the total accumulated heat until 150 h of T1 reaches the similar value as that of the control sample, suggesting that TA's retarding effect will diminish with the hydration process of alite.

The retarding effect of TA becomes stronger with 0.3% TA added. As revealed by the T3 curve in Fig. 2, the duration of the induction period of T3 is similar to T1. Its heat rate peak, however, is reduced by 20% compared to the control paste. More interestingly, after first acceleratory and deceleration periods, a second acceleratory and deceleration periods appear without an induction period [59]. The peak thermal power in the first acceleratory period is reduced by TA to just 10% of the control one and a new peak appeared at 61 h after the first thermal power peak at about 25.5 h, revealing the strong retarding effect of TA on the hydration of C_3S. In addition, a relatively high heat releasing rate can be observed until 120 h, indicating that the hydration kinetic is altered by the presence of TA.

The retarding effect of the TA is most severe when the TA content is increased to 0.5%. As shown in Fig. 2, the thermal power curve of T5 sample exhibits similar features as the T3 one. Consequently, the accumulated heats produced by the hydration until 150 h are reduced to 99%, 97%, and 68% by adding 0.1%, 0.3%, and 0.5% TA, respectively, compared to that of the control sample. Since the hydration degrees of the samples can be calculated by dividing their total released heats by the complete hydration heat of alite

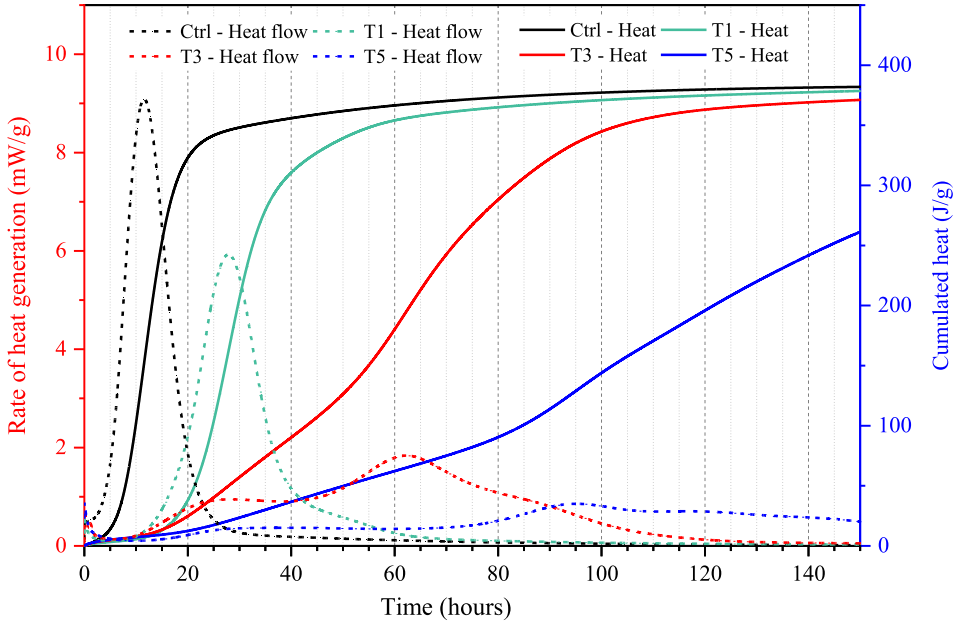

Fig. 2. Heat evolution of hydration in C_3S system with and without tannic acid.

(517 J/g), Fig. 2 shows that TA does reduce the degree of hydration of C_3S at early age (≤7d), but no obvious effect on the hydration degree in the long term.

According to the calorimetry data, the hydration kinetics are changed by the presence of TA. The BNG model was thus utilized to generate the quantitative description of this hydration processes. Because the shapes of the heat evolution for T3 and T5 have been completely altered, only the data of T1 and the control sample were analysed via the BNG model. Fig. 3 illustrates the fitted calorimetric data of the hydration of alite by assuming that C—S—H grows with constant nucleation rate or from constant number of nuclei. Table 2 summarizes the fitting parameters obtained from the BNG model.

Fig. 3(a) and 3(b) compare the testing data and their BNG model fitting based on the constant rate of nucleation assumption. Poorer fitting is achieved by the BNG model for T1 sample, suggesting that rate of nucleation must be altered by the addition of TA. More information on the retarding effect of TA can be observed from the fitting parameters: the fitting growth rate of T1 was reduced from 0.03245 to 0.0199 μm/h, and the nucleation rate was increased from 0.2025 to 0.2465 $(\mu m^{-2}h)^{-1}$. This indicates that TA can inhibit the growth, but promotes the nucleation rate of C—S—H. The increased induction time induced by TA also agrees with the calorimetric data. Similar features can be observed for the BNG fittings based on a constant number of nuclei for the samples, as shown in Fig. 3(c) and 3(d). The fitting growth rate of T1 was reduced from 0.03685 to 0.2575 μm/h, and the number of nuclei was increased from 2.21 to 2.85 μm^{-2}. It suggests that TA can facilitate the generation of nuclei for C—S—H formation, which agrees with the results obtained by BNG model with a constant nucleation rate.

3.2. AAS & pH

The total amount of calcium ions in the pore solution of alite was determined by atomic absorption spectroscopy (AAS), as shown in Fig. 4(a). The calcium ions concentration in the pure C_3S pore solution (Fig. 4(a)) exhibits four periods corresponding to that of the micro-calorimetry result (Fig. 2(a)). In the initial period, the concentration of Ca^{2+} increases quickly to reach oversaturation due to the dissolution of C_3S in the water. In the second period (induction period), hydration products start to precipitate due to the oversaturation of the Ca^{2+}. In this period, the precipitated Ca^{2+} and the new Ca^{2+} dissolved from C_3S seem to reach a balance. As a result, the concentration of Ca^{2+} is almost a constant in this period. After that, the concentration of Ca^{2+} reduces quickly

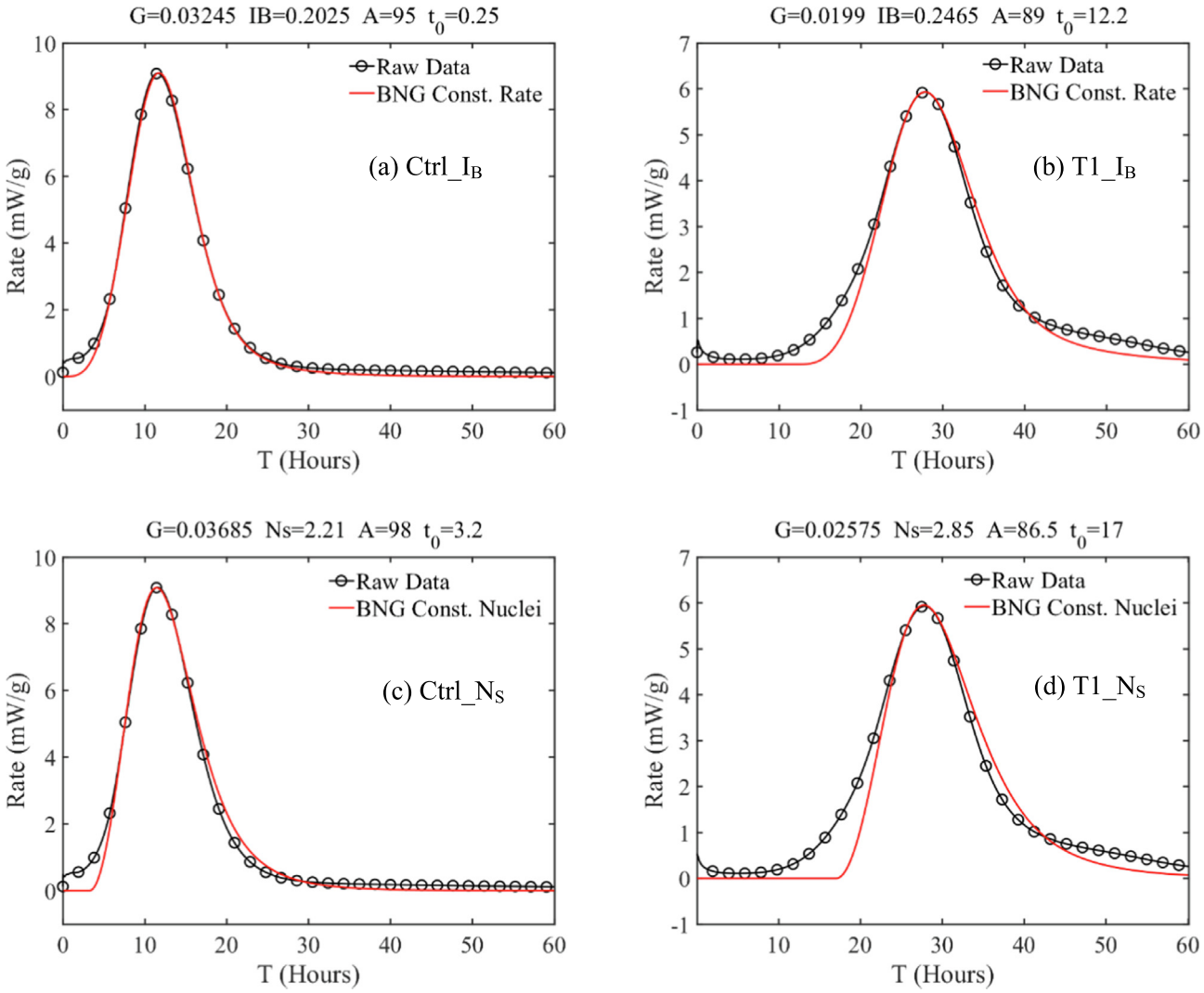

Fig. 3. Fitted calorimetric data for hydration of alite in presence of TA or not, assuming growth with constant nucleation rate (a&b) or from constant number of nuclei (c&d). The parameters used here are presented in Table 2.

Table 2
Fitting parameters obtained with the BNG models.

BNG	Sample	G (μm/h)	I_B ($\mu m^{-2}h)^{-1}$	N_S (μm^{-2})	A (kJ/mol)	t_0 (h)
Constant Nucleation Rate	Ctrl	0.03245	0.2025	–	95.0	0.25
	T1	0.0199	0.2465	–	89.0	12.20
Constant Number of Nuclei	Ctrl	0.03685	–	2.21	98.0	3.20
	T1	0.02575	–	2.85	86.5	17.00

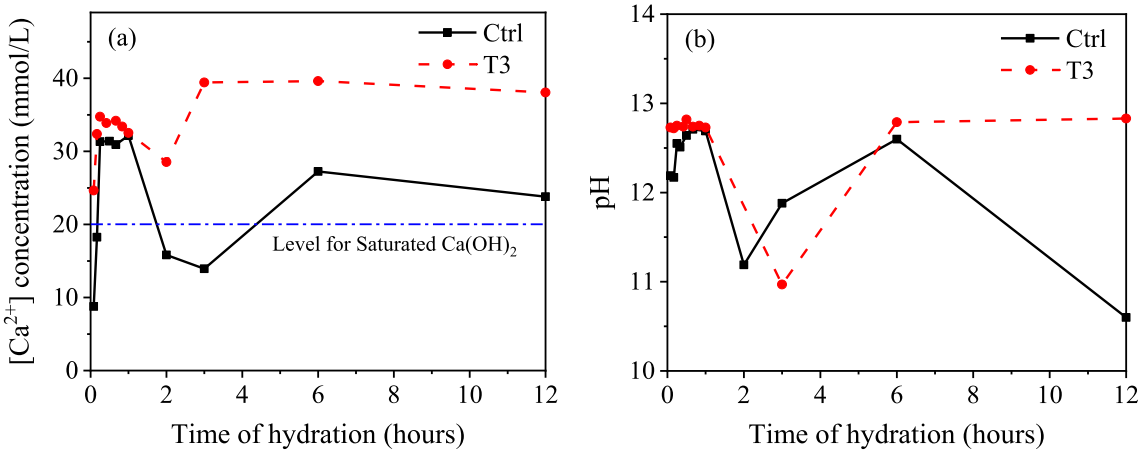

Fig. 4. The total release of calcium and alkali ions into solution during the hydration of alite at different ages: (a) calcium concentration; (b) pH of the obtained solution.

with the hydration time, suggesting that acceleratory period starts [60,61]. At the beginning of this period, oversaturated Ca^{2+} precipitates quickly into the hydration products such that its concentration level is even below the saturation point. Consequently, more Ca^{2+} can be dissolved into the pores, raising the Ca^{2+} concentration slightly above the saturation point for CH.

After adding TA, these four periods are still there, as shown in Fig. 4(a). However, the concentration of Ca^{2+} in all these periods is significantly higher than that in the control sample. This can be clearly attributed to the calcium chelate complex in the pore solution induced by TA molecules. The phenolic carboxylic or hydroxyl groups in TA can interact with calcium and form a strong chelate complex with calcium [62–65]. The chelate complex typically reduced the activity of the calcium ions. The chelate complex and insoluble salts required more calcium dissolved to saturate the solution with respect to CH.

The alkali level of the pore solution measured by a pH meter is shown in Fig. 4(b), which exhibits the same four periods as that of the calcium ions. Addition of TA slightly changed this curve. One interesting feature is that the pH value of the pore solution was even slightly higher after adding TA. This suggests that the addition of TA does not impair the alkaline environment in the pore solution, which is critical to protect the reinforcing steel in the concrete. A sharp decrease of the pH value in the control sample at 12 h could be induced by experimental error or carbonation by CO_2 from air. Further study will be carried out to clarify this.

The chelate reaction between TA and calcium ions in the pore solution can be further verified by FTIR spectra shown in Fig. 5. In this figure, pore solution is produced by mixing pure CH with TA solution at 1% of the mass of CH for 30 mins and stirring the slurry for 30 mins. The reaction products were filtered out and washed with ethanol. FTIR spectra of the hydration products and the pure CH were obtained by employing KBr disc technique from 400 cm^{-1} to 2000 cm^{-1}, as shown in Fig. 5. The typical bonds of TA are in-plane bending of —OH located at 1070–1200 cm^{-1}, the peak of —C=C— located at 1365–1578 cm^{-1}, and the vibration of —C—O— near 1652 cm^{-1} [66]. It can be seen that the typical bonds of TA (—OH, —C=C—, —C—O—) in group CH + TA were shifted compared that in TA, which indicates the strong chelate reaction between TA and calcium ions [65], which is also confirmed by a molecular dynamics simulation [67].

3.3. Hydration products of alite

3.3.1. XRD

Fig. 6 presents the XRD patterns of the C_3S pastes with and without TA at different ages. In addition to unhydrated alite, the crystallized hydration product CH could be identified from the patterns. The XRD results could not reveal any changes in mineral compositions due to the addition of TA. The XRD patterns of pastes with and without TA showed no difference after 3 h curing, as shown in Fig. 6(a) and 6(b). The retarding effect of TA can be clearly

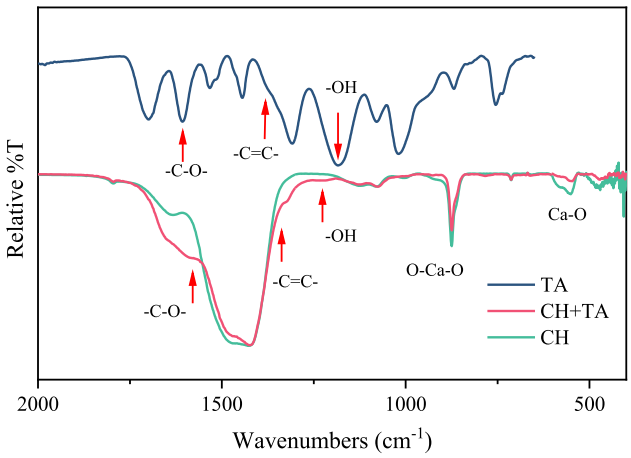

Fig. 5. FTIR spectra of the reacted products of TA and CH.

observed from Fig. 6(c) and 6(d), which indicates that the intensity of the peaks of C_3S of the sample increasing with the concentration of TA, which is consistent with the results shown in the micro-calorimetry test.

It should be mentioned that the ratio between different peaks of CH is affected by the addition of TA, as shown in Fig. 6(e) and 6(f). After 28d curing, the peak of CH at 21° ([001]) is significantly higher than the peak of CH at 40° ([101]) in the specimens prepared with TA. This suggests that CH crystal prefers to grow along its c-axis [68] and has high crystallinity in the face [001].

According to Grandet and Ollivier [69], the orientation index of CH can be defined as:

$$\text{Orientation index} = \frac{\text{intensity}(001)}{\text{intensity}(101) \times 0.74} \tag{9}$$

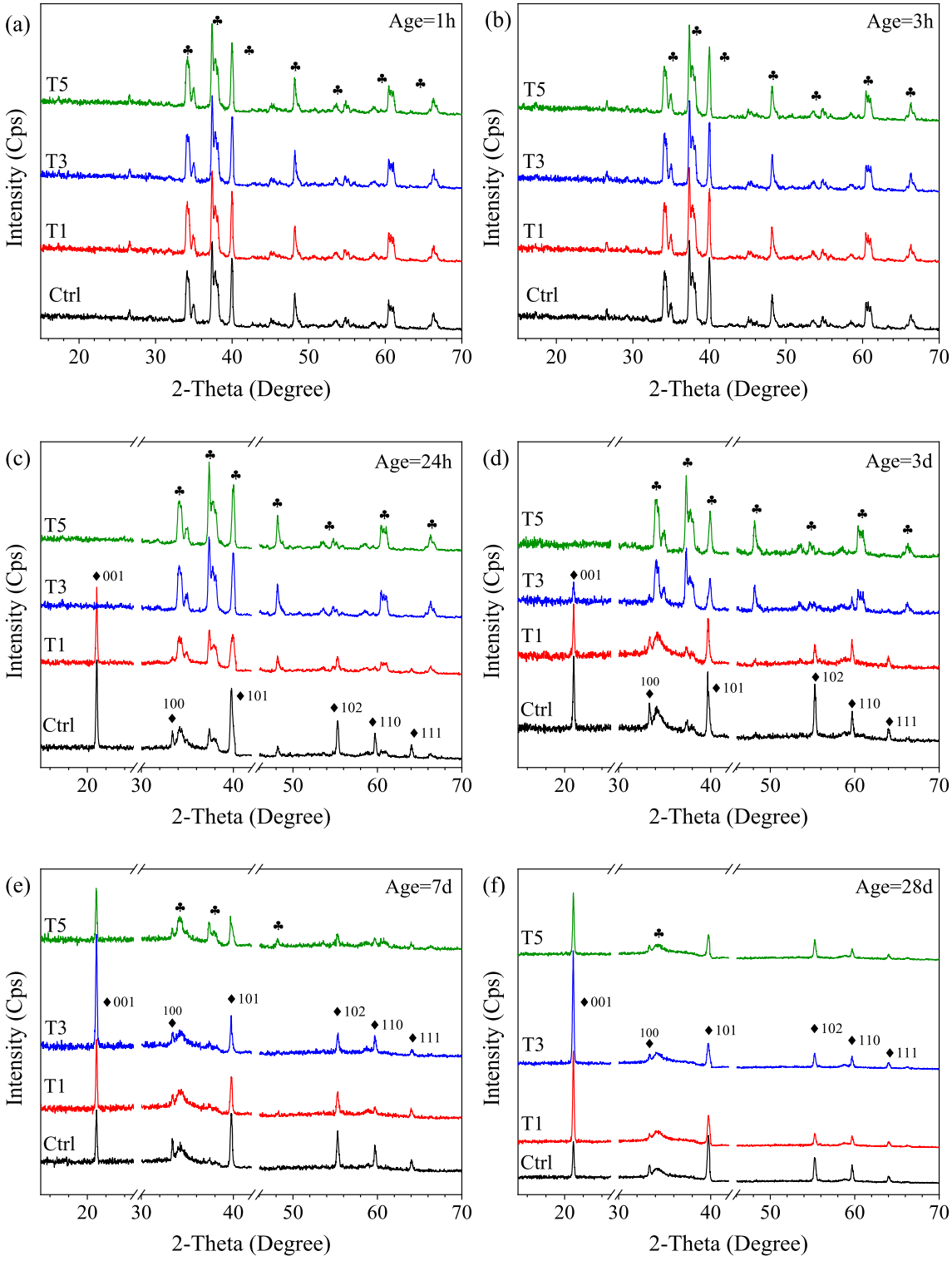

Fig. 6. XRD patterns of hydration products of alite modified with TA at different curing ages (♣: tricalcium silicate C_3S; ◆: portlandite CH): (a) 1 h, (b) 3 h, (c) 24 h, (d) 3 days, (e) 7 days, and (f) 28 days.

The CH crystals exhibit random orientation and the ratio between the heights of the 2-theta equals 21° ([001]), and 2-theta equals to 40° ([101]) peak heights is close to 0.74, which is the ratio obtained from the standard portlandite samples. High orientation index means more crystals orientated with their c-axis.

As Fig. 7 shows, the orientation index of the control group decreases with the curing age increasing. In the absence of TA, CH generates preferentially on the [001] face causing prismatic habits along the c-axis initially [60]. But in the later time, growth of CH occurs on the other faces at relatively lower calcium ions concentrations, reducing the orientation index. This trend is altered by the presence of TA. As shown in Fig. 7, the orientation index of CH increases with the age, rather than decreasing to one. Moreover, higher orientation index was achieved by using more TA, except for the 0.5% TA sample. The high dosage of TA (0.5%) seriously retarded the hydration and consumes more CH during the hydration, thus reduce the orientation index of CH comparing to that of the group with 0.3% TA.

3.3.2. TGA

TGA and DTG were employed to quantitatively analyse the hydration products, as shown in Fig. S2 (see Supplementary Material). The quantification of hydration products and bound water of alite at different curing ages were calculated based on the weight loss in the assigned temperature intervals, and the results were shown in Fig. 8. As shown in Fig. 8(a), adding 0.1% TA into the paste produces more C—S—H at 3d, suggesting a higher degree of hydration is reached. However, the content of portlandite in this sample at 3d is not increased accordingly, as shown in Fig. 8(b). With more TA added, both the C—S—H and CH are reduced at 3d, due to the stronger retarding effect. However, after curing for 7d, the C—S—H contents in all pastes with TA are close to that of the control group, indicating the retarding effect of the TA almost diminished after 7d hydration. As expected, CH contents in these samples decrease with the increase of the TA content. The C—S—H content of the sample with 0.5% TA at 7d is surprisingly higher than that of T3, which can be induced by the decomposition of more calcium chelate. When the curing age reached 28d, the contents of C—S—H are increased by 2.0%, 7.7%, and 6.1% with addition of TA at 0.1%, 0.3%, and 0.5%, respectively.

The degree of hydration of the alite paste can be determined by the content of bound water, as shown in Fig. 8(c). This figure shows that a TA doped pastes reached a lower degree of hydration than the control paste in the early ages (3d and 7d) due to the retarding effect of the TA. At 28d, however, all pastes reached a similar degree of hydration. Therefore, the increase of the C—S—H in TA doped pastes was resulted from TA converting some CH into C—S—H, most likely through incorporating more calcium in C—S—H through TA-calcium complex. This can be confirmed by the content of CH in all pastes at 28d shown in Fig. 8(b), which revealed that the contents of CH in T1, T2 and T3 paste were decreased by 5.2%, 9.5%, and 13.7%, respectively, at 28d. According to the reaction formula (5), the total amounts of calcium and silica in the hydration products are directly related to the degree of hydration, or the bound water. With similar degree of hydration, the increased amount of C—S—H indicates a higher Ca/Si ratio of C—S—H. Therefore, TA doping increases the Ca/Si ratio of the C—S—H. This is not surprising since the concentration of Ca^{2+} is higher in the pore solution of the paste with TA, as revealed by Fig. 4. Previous study found that C—S—H grains with a higher Ca/Si ratio are packed in a denser microstructure with a smaller grains unit [54].

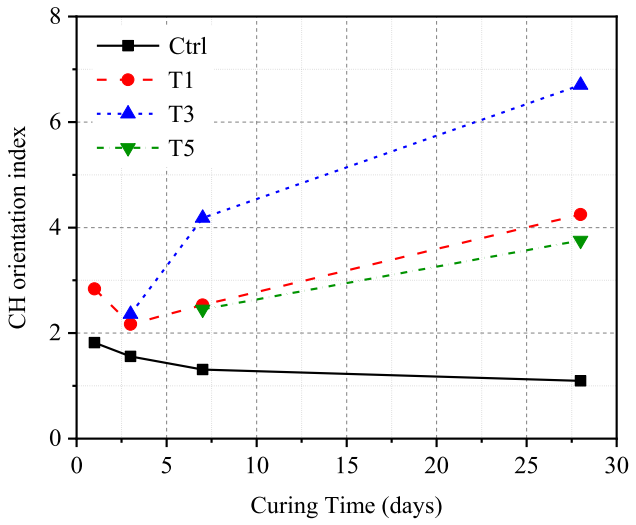

Fig. 7. The effect of TA on the CH orientation index of hydrated alite pastes.

3.3.3. FTIR

FTIR spectra were used to further examine modification of the structure of C—S—H induced by TA, as shown in Fig. S3 (see Supplementary Material). In this figure, the signal around 810 cm^{-1} is related to Si single bond O stretching of Q1 tetrahedra [52,70], while the main peak of the FTIR spectra located between 940 and 960 cm^{-1} has often been assigned in the literature to Q2 vibrations [52,70]. The intensity of Q^1 represents the amount of end silicate tetrahedra and the intensity of Q^2 corresponds to the amount of the bridging silicate tetrahedra [49]. The mean chain length (MCL) is computed based on the peak intensity ratio of the Q^1 and Q^2 signal as described in the Materials and Methods chapter. Fig. 9 shows that the MCL increases with the curing time. The reduction of MCL after 7d was induced by the inevitable moisture evaporation, even in the sealed environment. It can be seen that MCLs of the C—S—H in the TA doped samples are shorter than that of the C—S—H in the control sample. It is also shown that the MCL decreases with the increase of the concentration of TA doping.

3.3.4. ^{29}Si MAS NMR

^{29}Si MAS NMR was carried out on the alite hydrates with or without TA to confirm the finding revealed by FTIR, as shown in Fig. S4 (see Supplementary Material). The computed lengths of silica chains based on NMR spectra [45,52] are presented in Fig. 10, together with the ones obtained from the FTIR spectra. MCL calculated from FTIR was larger than that obtained from NMR results for all ages. In addition, MCL increases with the curing time and reduces with the presence of TA, agreeing with the results obtained from the FTIR spectra. Therefore, FTIR can be used as a convenient alternative for NMR to study the C—S—H structure.

3.4. Pore structure

Fig. 11 compares the pore structures of the C_3S pastes at 28d prepared with w/b = 1 and without (Ctrl) and with 0.3%TA added (T3) obtained by MIP. Two peaks can be identified on the pore size distribution curve of the alite paste without TA, located at 340 nm and 30 nm. After adding 0.3% TA to the paste, the peak at 30 nm is almost eliminated by the TA, suggesting that TA has a unique ability to radically reduce these inter-hydrate pores. This provides direct evidence that TA has ability to densify the nanoscale structure of the hydration products of alite, which is of great importance and can be the major reason responsible for the significant improvement on the compressive strength of concrete induced by TA.

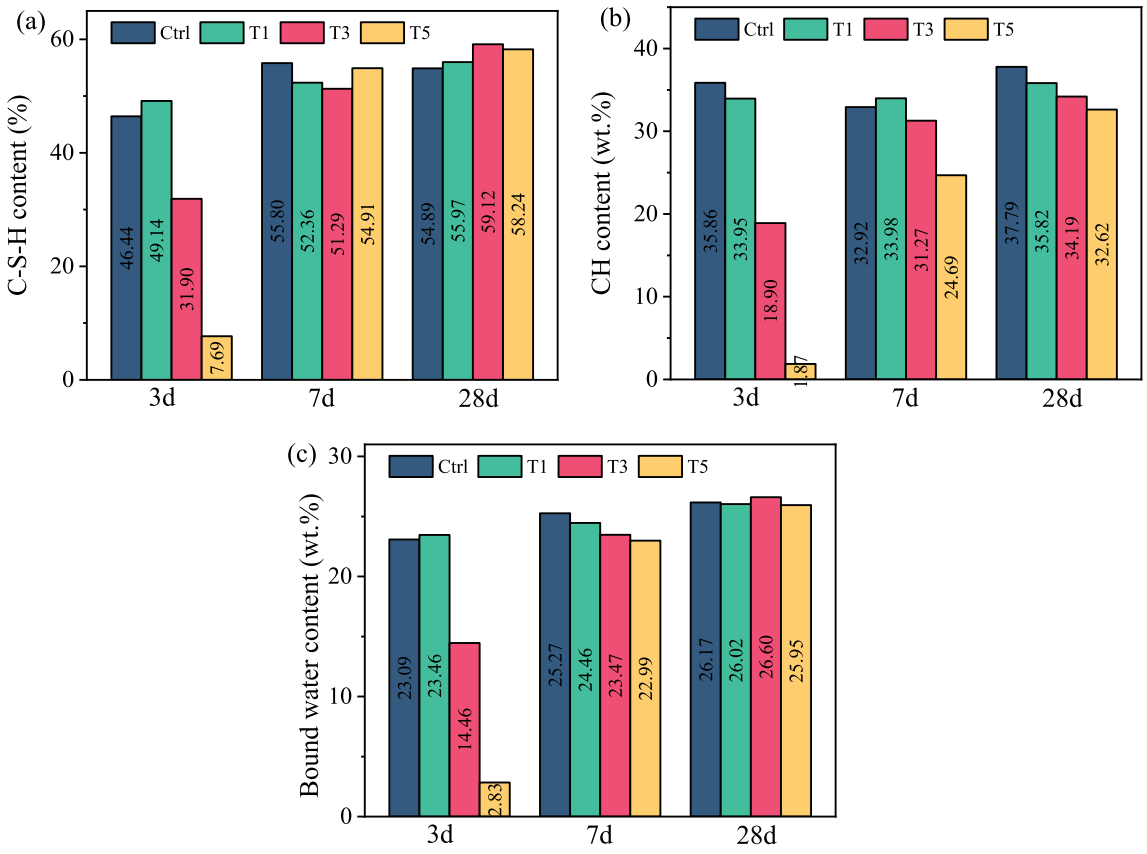

Fig. 8. Quantification of hydration products and bound water of alite at different curing ages: (a) CSH, (b) CH, (c) Bound water.

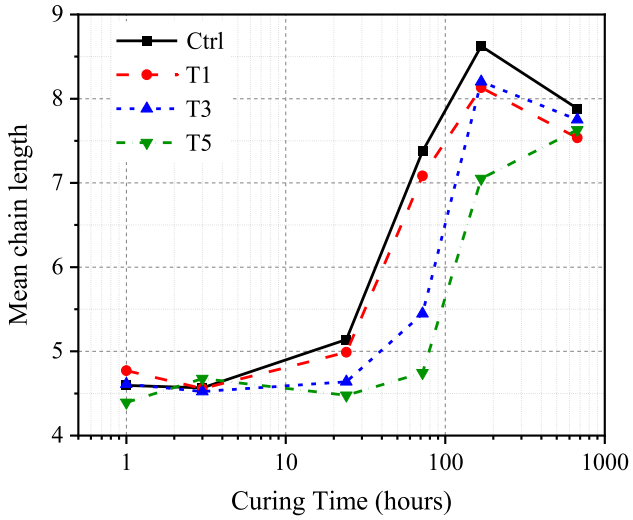

Fig. 9. Mean chain length changes of C—S—H induced by TA doping calculated based on the FTIR spectra.

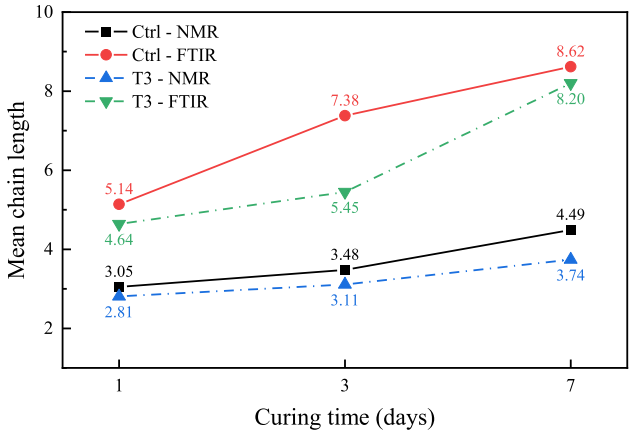

Fig. 10. Calculated MCL values based on ^{29}Si Solid NMR and FTIR results.

3.5. Nanomechanical properties

Elastic moduli of C—S—H obtained by nanoindentation are shown in Fig. 12(a) and 12(b). It can be seen that the average elastic modulus of the C—S—H was increased from 24.34 GPa in the Ctrl paste to 25.79 GPa in the paste added with 0.3% TA. Since there is a linear relationship between the elastic modulus and packing density, the corresponding packing density was enhanced from 0.702 to 0.716 by the presence of TA, as shown in Fig. 12(c) and 12(d). This agrees very well with the MIP result shown in Fig. 11, confirming that the interactions including hydrogen and ionic bonds induced by TA can densify the nanoscale hydration products and reduce nanopores in the paste, leading to higher elastic modulus and packing density.

By deconvoluting the measured elastic moduli shown in Fig. 12, three phases of hydration products (excluding anhydrous clinker minerals) can be identified, which are low density C—S—H (LD), high density C—S—H (HD), and an ultra-high density C—S—H (UHD), in the order of the lowest to highest elastic moduli. In this figure, π, μ and σ are the volume fraction, the mean value (in GPa), and the standard deviation (in GPa) of each phase, respectively. Although TA can enhance the overall elastic modulus of the hydra-

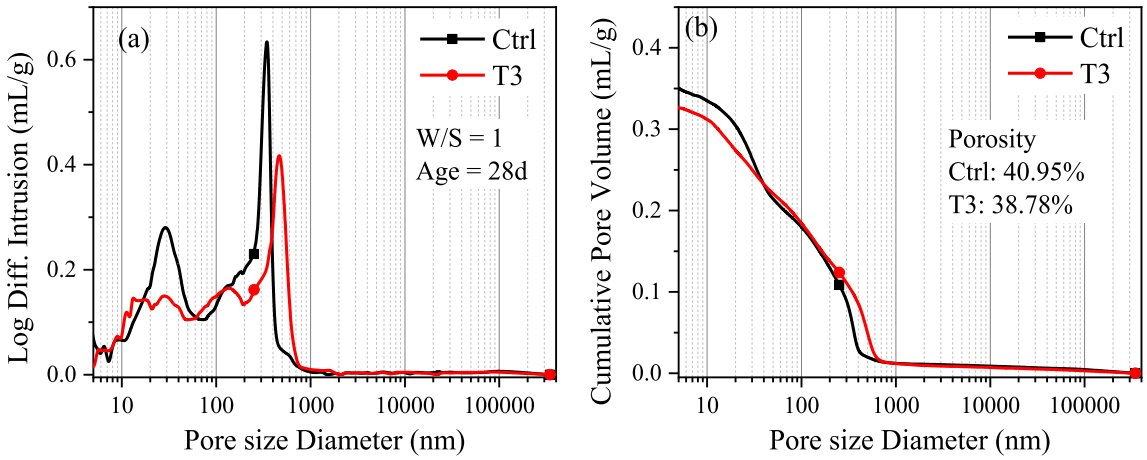

Fig. 11. Pore size distribution of alite pastes modified by TA: (a) Log differential intrusion; (b) Cumulative intrusion.

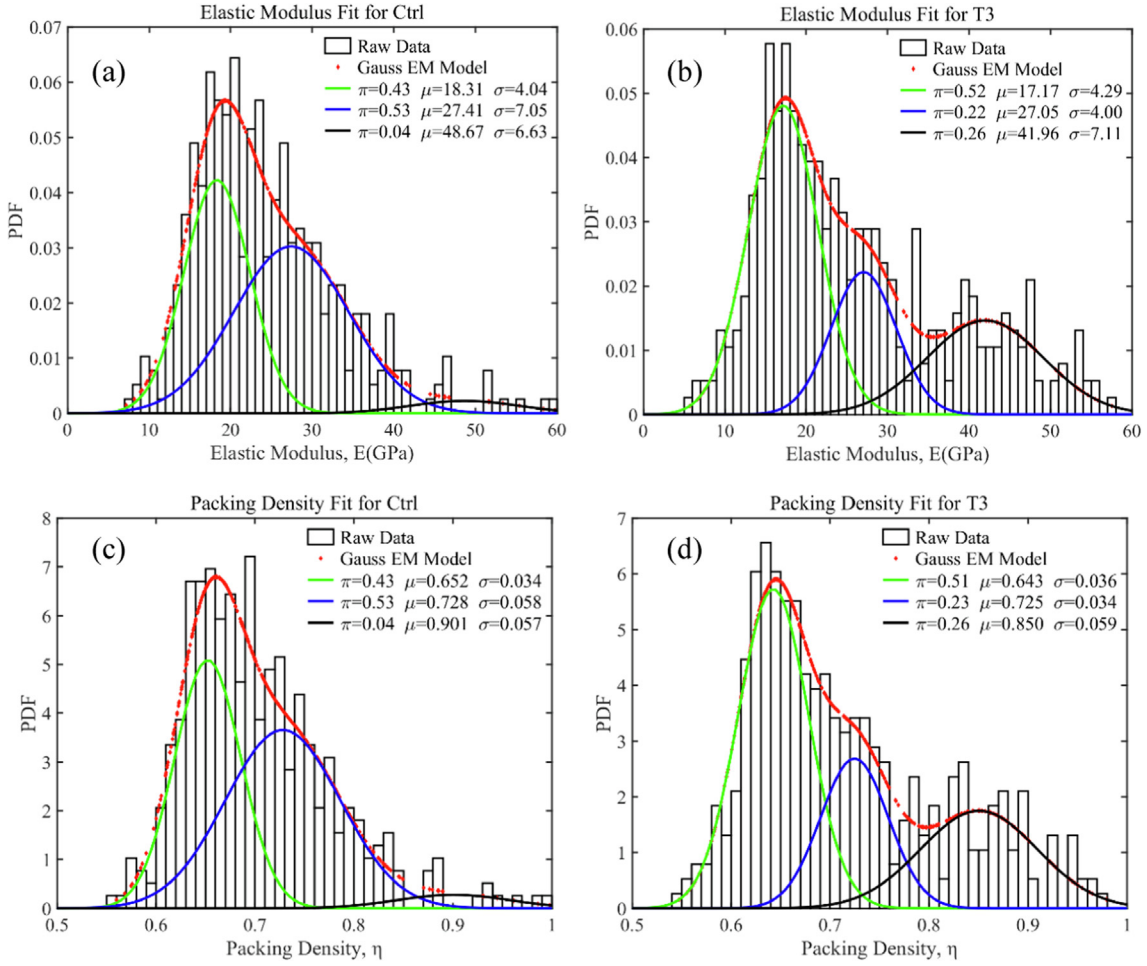

Fig. 12. Deconvolution results of elastic modulus (E) and packing density (η) of grid of nanoindentation (20 × 20 grids): (a) The elastic modulus for Ctrl; (b) The elastic modulus for T3; (c) The packing density for Ctrl; and (d) the packing density for T3.

tion products, its effect on individual phases are obviously affected differently. Volume ratios of LD C—S—H, HD C—S—H and UHD C—S—H were changed by the addition of TA from 43% to 52%, 53% to 22%, 4% to 26%, respectively, in comparison with that of the control sample. Existing study suggests that UHD C—S—H is essentially nanocomposite of C—S—H and CH [63]. More UHD C—S—H produced implies that the presence of TA induces more CH nanoparticles co-precipitating with C—S—H and fill some inter-hydrate nanopores between C—S—H grains. This may be another reason responsible for the drastic reduction of the pores with size around 30 nm in the TA-doped paste revealed by Fig. 11. On the other hand, more LD C—S—H can increase the volume of the hydration products, leading to reduction of porosity of the alite paste, as revealed by Fig. 11(b).

4. Discussions

This study aimed to provide a preliminary insight into the effect of TA on the hydration of alite paste and the major hydration products, especially C—S—H, thus exploring the mechanisms responsible for the enhanced performance of the concrete induced by doping TA. It was found that the total accumulated heat until 150 h was reduced subsequently as the TA concentration increased, suggesting that TA has a strong retardation effect on the hydration of alite. In addition, the induction period is extended significantly in the presence of TA. This is because TA molecules can be adsorbed on the surface of alite grains and the phenolic carboxylic or hydroxyl groups in TA can form a strong chelate complex with calcium [29,65], which was verified by the shift of typical bonds of TA as shown in FTIR spectra. The latter would also reduce the activity of the calcium ions and cause the reduction of the available free calcium ions to form hydration products. This can be seen from the higher calcium ions concentrations in the pore solution of alite slurry, as shown in Fig. 4(a). The produced chelated calcium ions can also be adsorbed onto the growth sites on alite particle normally occupied by free calcium ions, thereby 'poisoning' the growth sites [60]. According to XRD data, TA causes CH to grow preferentially on the [001] face due to the calcium chelate's adsorption on CH, which results in prismatic behaviour along the c-axis. This is because the chelated calcium ions can be adsorbed onto the [001] face during the hydration, preventing the growth on the other faces. Such a significant change on the growth pattern of CH induced by TA will inevitably affect the mechanical properties and chemical stability of CH.

The BNG results showed that the nucleation rate of T1 was increased from 0.2025 to 0.2465 $(\mu m^{-2}h)^{-1}$ and the number of nuclei of T1 was increased from 2.21 to 2.85 μm^{-2}. This indicates that TA would inhibit the growth, but promotes the nucleation rate of C—S—H or facilitate the generation of nuclei for C—S—H formation. The mechanism of this occurrence could be that the produced calcium chelates in induction period served as nuclei for the growth of C—S—H. In addition, this process could achieve the organic–inorganic hybridization of C—S—H [5], which is to graft small organic groups or polymeric chains into growing C—S—H phase to achieve covalent hybridization. TGA results showed that the increase of TA concentration induced the decrease of the CH content and the increase of C—S—H. However, the degree of hydration of the hydration product at 28d was similar, which indicated that TA could convert part of CH into organic–inorganic hybridized C—S—H. The hybridization will result in the increase of Ca/Si of C—S—H due to the existing of calcium chelate in C—S—H layers.

Existing studies [71,72] also revealed that the MCL of C—S—H generally reduces with the increase of the Ca/Si, which agrees with the results obtained from FTIR and NMR. This reduction of the MCL can be attributed to the TA-Ca^{2+} complexes, which elevate the concentration of calcium ions in the pore solution (Fig. 4) and seed the C—S—H formation (Fig. 3). The presence of more calcium chelates in the structure tends to decrease the space for silicates tetrahedra to form longer chains. It is of great significance to be able to tune the MCL of C—S—H because the mechanical properties of the cementitious material can be subsequentially changed. By using high pressure X-ray diffraction to measure the intrinsic nanomechanical properties of C—S—H, Li et al. [73] demonstrated that higher Ca/Si leads to higher mechanical properties for the C—S—Hs prepared by coprecipitation. In addition, previous study also found that C—S—H grains with a higher Ca/Si ratio are packed in a denser microstructure with a smaller grains unit [54]. This is consistent with the nanoindentation results as shown in Fig. 12. Compared with the Ctrl paste, much less HD C—S—H and much more UHD C—S—H were produced in the T3 paste. Therefore, TA provides a simple way to tune the hydration product at atomic level to achieve desirable structural and mechanical properties of cementitious materials.

It was also observed that TA can significantly change the pore structures of the hardened paste. Particularly, capillary pores smaller than 70 nm are drastically reduced by adding TA, as revealed by MIP results. This is of great importance and can be the major reason responsible for the significant improvement on the compressive strength of concrete induced by TA. The reduction of the inter-hydrate pores can be attributed to TA's ability to bind to or crosslink hydration products through multiple interactions, especially hydrogen and ionic bonds. These interactions provide extra adhesion to densify the loose nanoscale hydration products to form denser and larger grains. Since denser hydration products occupy smaller amount of space, large capillary pores peak at 340 nm are enlarged by the presence of TA with a new peak at 480 nm, as shown in Fig. 11. This may be detrimental to the strength of the concrete, which is undesirable. However, adverse effect is offset by the drastic reduction of the small pores. This has been confirmed by existing studies [35,37,38] which show the compressive strength of the cement mortars can be significantly improved by adding TA.

5. Conclusions

This study exploits a mussel-inspired biomolecule, TA to tune the hydration of alite. A comprehensive experimental program has been carried out, based on which, the following conclusions can be draw:

1) TA has a strong retardation effect on the hydration of alite due to its ability to bind to alite particles and to chelate calcium ions. The chelation consumes the calcium ions in the solution, while the adsorption of organic molecules blocks the dissolution of alite. Nevertheless, this retarding effect can be mitigated by using appropriate accelerators. According to BNG models, TA can inhibit the growth rate of C—S—H, whereas promote the generation of nuclei for C—S—H formation, which can improve the microstructure of the hardened paste.
2) TA can significantly change the morphology of hydration products at early age. Particularly, spherical nanoparticles have been in-situ produced in the fresh alite paste at 1 h, resulted from the strong interactions between TA and the hydration products.
3) TA induces preferential growth of CH on the [001] face due to the adsorption of calcium chelate on CH, producing prismatic habits along the c-axis. The large surface area on the [001] face can adsorb numbers of calcium chelate complexes in the pore solution, producing more crystals orientated with their c-axis. This may have profound effect on the strength and durability of the produced concrete, and certainly deserves more research in the future.
4) TA can modify the atomic structure of C—S—H, as indicated by a higher Ca/Si ratio and reduced mean chain length of C—S—H measured by FTIR and NMR. This can be attributed to the formation of complex between TA and calcium, on which C—S—H grows.
5) TA can change the pore structures of the hardened paste. Particularly, capillary pores smaller than 70 nm are drastically reduced by adding TA, as revealed by MIP results. As a result, the elastic modulus of C—S—H obtained by nanoindentation testing is improved.

In conclusion, TA can modify all hydration products and their microstructures of alite due to its strong ability to interact with various materials. Particularly, TA can modify the pore structure of the hydration products of alite, offering a new tool to improve the performance of OPC-based concrete. Its unique molecule structure and function broadens the range of possibilities of traditional non-renewable admixtures. More importantly, its nature origin and many desirable features such as abundant, non-toxic, low/negative carbon, yet low-cost, make it an ideal candidate for next generation eco-friendly chemical admixture for concrete.

CRediT authorship contribution statement

Yi Fang: Methodology, Investigation, Visualization, Writing – original draft. **Jialai Wang:** Conceptualization, Funding acquisition, Supervision, Writing – review & editing. **Liang Wang:** Investigation. **Xin Qian:** Investigation, Supervision, Writing – review & editing. **Xiaodong Wang:** Investigation. **Wenyu Liao:** Investigation. **Peiyuan Chen:** Investigation. **Hongyan Ma:** Investigation, Writing – review & editing.

Data availability

Data will be made available on request.

Declaration of Competing Interest

The authors declare that they have no known competing financial interests or personal relationships that could have appeared to influence the work reported in this paper.

Acknowledgements

This study was partially supported by the National Science Foundation – United States (#1761672, #1761697, and #2236331), and the National Natural Science Foundation of China (52108187 and 51908418). Any opinions, findings, and conclusions, or recommendations expressed in this material are those of the author(s) and do not necessarily reflect those of the National Science Foundation.

Appendix A. Supplementary data

Supplementary data to this article can be found online at https://doi.org/10.1016/j.matdes.2022.111490.

References

[1] J.J. Biernacki, J.W. Bullard, G. Sant, K. Brown, F.P. Glasser, S. Jones, T. Ley, R. Livingston, L. Nicoleau, J. Olek, Cements in the 21st century: challenges, perspectives, and opportunities, J. Am. Ceram. Soc. 100 (7) (2017) 2746–2773.
[2] G. Habert, S.A. Miller, V.M. John, J.L. Provis, A. Favier, A. Horvath, K.L. Scrivener, Environmental impacts and decarbonization strategies in the cement and concrete industries, Nat. Rev. Earth & Environ. 1 (11) (2020) 559–573.
[3] G. Hammond, C. Jones, Inventory of carbon & energy (ICE) version 3.0, University of Bath, 2019
[4] G. Constantinides, F.-J. Ulm, The nanogranular nature of C-S–H, J. Mech. Phys. Solids 55 (1) (2007) 64–90.
[5] R.-M. Pellenq, N. Lequeux, H. Van Damme, Engineering the bonding scheme in C-S–H: The iono-covalent framework, Cem. Concr. Res. 38 (2) (2008) 159–174.
[6] M. Vandamme, F.-J. Ulm, P. Fonollosa, Nanogranular packing of C-S–H at substochiometric conditions, Cem. Concr. Res. 40 (1) (2010) 14–26.
[7] M. Vandamme, F.-J. Ulm, Nanogranular origin of concrete creep, Proceedings of the National Academy of Sciences 106(26) (2009) 10552-10557.
[8] M.J.A. Qomi, F.-J. Ulm, R.-J.-M. Pellenq, Physical origins of thermal properties of cement paste, Phys. Rev. Appl. 3 (6) (2015) 064010.
[9] Y. Zhou, A. Morshedifard, J. Lee, M.J. Abdolhosseini Qomi, The contribution of propagons and diffusons in heat transport through calcium-silicate-hydrates, Appl. Phys. Lett. 110 (4) (2017) 043104.
[10] M.J. Abdolhosseini Qomi, F.J. Ulm, R.J.M. Pellenq, Evidence on the dual nature of aluminum in the calcium-silicate-hydrates based on atomistic simulations, J. Am. Ceram. Soc. 95 (3) (2012) 1128–1137.
[11] Y. Zhou, D. Hou, J. Jiang, W. She, J. Yu, Reactive molecular simulation on the calcium silicate hydrates/polyethylene glycol composites, Chem. Phys. Lett. 687 (2017) 184–187.
[12] Y. Zhou, L. Tang, J. Liu, C. Miao, Interaction mechanisms between organic and inorganic phases in calcium silicate hydrates/poly (vinyl alcohol) composites, Cem. Concr. Res. 125 (2019) 105891.
[13] Y. Zhou, C.A. Orozco, E. Duque-Redondo, H. Manzano, G. Geng, P. Feng, P.J. Monteiro, C. Miao, Modification of poly (ethylene glycol) on the microstructure and mechanical properties of calcium silicate hydrates, Cem. Concr. Res. 115 (2019) 20–30.
[14] Y. Zhou, D. Hou, H. Manzano, C.A. Orozco, G. Geng, P.J. Monteiro, J. Liu, Interfacial connection mechanisms in calcium–silicate–hydrates/polymer nanocomposites: a molecular dynamics study, ACS Appl. Mater. Interfaces 9 (46) (2017) 41014–41025.
[15] F. Sanchez, L. Zhang, Molecular dynamics modeling of the interface between surface functionalized graphitic structures and calcium–silicate–hydrate: interaction energies, structure, and dynamics, J. Colloid Interface Sci. 323 (2) (2008) 349–358.
[16] A. Moshiri, D. Stefaniuk, S.K. Smith, A. Morshedifard, D.F. Rodrigues, M.J.A. Qomi, K.J. Krakowiak, Structure and morphology of calcium-silicate-hydrates cross-linked with dipodal organosilanes, Cem. Concr. Res. 133 (2020) 106076.
[17] J.H. Waite, Nature's underwater adhesive specialist, Int. J. Adhes. Adhes. 7 (1) (1987) 9–14.
[18] J.H. Waite, M.L. Tanzer, Polyphenolic substance of Mytilus edulis: novel adhesive containing L-dopa and hydroxyproline, Science 212 (4498) (1981) 1038–1040.
[19] Q. Guo, J. Chen, J. Wang, H. Zeng, J. Yu, Recent progress in synthesis and application of mussel-inspired adhesives, Nanoscale 12 (3) (2020) 1307–1324.
[20] E. Faure, C. Falentin-Daudré, C. Jérôme, J. Lyskawa, D. Fournier, P. Woisel, C. Detrembleur, Catechols as versatile platforms in polymer chemistry, Prog. Polym. Sci. 38 (1) (2013) 236–270.
[21] N. Zohhadi, Bio-Inspired and Low-Content Polymer Cement Mortar for Structural Rehabilitation, University of South Carolina - Columbia, Retrieved from https://scholarcommons.sc.edu/etd/2687, 2014
[22] Y. Fang, J. Wang, X. Qian, L. Wang, G. Lin, Z. Liu, Bio-inspired functionalization of very fine aggregates for better performance of cementitious materials, Constr. Build. Mater. 241 (2020) 118104.
[23] G.R. Jenness, M.K. Shukla, Effect of Concrete Composition on the Thermodynamic Binding of Dopamine: A DFT Study, Langmuir (2021).
[24] Q. Wei, R. Haag, Universal polymer coatings and their representative biomedical applications, Mater. Horiz. 2 (6) (2015) 567–577.
[25] F. Heijmen, J. Du Pont, E. Middelkoop, R. Kreis, M. Hoekstra, Cross-linking of dermal sheep collagen with tannic acid, Biomaterials 18 (10) (1997) 749–754.
[26] T. Shutava, M. Prouty, D. Kommireddy, Y. Lvov, pH responsive decomposable layer-by-layer nanofilms and capsules on the basis of tannic acid, Macromolecules 38 (7) (2005) 2850–2858.
[27] I. Erel-Unal, S.A. Sukhishvili, Hydrogen-bonded multilayers of a neutral polymer and a polyphenol, Macromolecules 41 (11) (2008) 3962–3970.
[28] A.E. Hagerman, K.M. Riedl, G.A. Jones, K.N. Sovik, N.T. Ritchard, P.W. Hartzfeld, T.L. Riechel, High molecular weight plant polyphenolics (tannins) as biological antioxidants, J. Agric. Food Chem. 46 (5) (1998) 1887–1892.
[29] S.R. Abulateefeh, M.O. Taha, Enhanced drug encapsulation and extended release profiles of calcium–alginate nanoparticles by using tannic acid as a bridging cross-linking agent, J. Microencapsul. 32 (1) (2015) 96–105.
[30] A. Hadfi, I. Karmal, B.E. Ibrahimi, S. Ben-aazza, M. Errami, S. Mohareb, A. Driouiche, Experimental investigation and molecular dynamic simulation of Tannic acid as an eco-friendly inhibitor for calcium carbonate scale, J. Mol. Liq. 340 (2021) 117225.
[31] H. Shagholani, S.M. Ghoreishi, Investigation of tannic acid cross-linked onto magnetite nanoparticles for applying in drug delivery systems, J. Drug Delivery Sci. Technol. 39 (2017) 88–94.
[32] I. Keita, B. Sorgho, C. Dembele, M. Plea, L. Zerbo, B. Guel, R. Ouedraogo, M. Gomina, P. Blanchart, Ageing of clay and clay–tannin geomaterials for building, Constr. Build. Mater. 61 (2014) 114–119.
[33] B. Sorgho, L. Zerbo, I. Keita, C. Dembele, M. Plea, V. Sol, M. Gomina, P. Blanchart, Strength and creep behavior of geomaterials for building with tannin addition, Mater. Struct. 47 (6) (2014) 937–946.
[34] Y. Du, C. Brumaud, F. Winnefeld, Y.-H. Lai, G. Habert, Mechanisms for efficient clay dispersing effect with tannins and sodium hydroxide, Colloids Surf. A 630 (2021) 127589.
[35] Y. Fang, J. Wang, X. Qian, L. Wang, Y. Dong, P. Qiao, Low-cost, ubiquitous biomolecule as a strength enhancer for cement mortars, Constr. Build. Mater. 311 (2021) 125305.
[36] Y. Fang, Low-cost, ubiquitous biomolecule as next generation, sustainable admixture to enhance the performance of ordinary portland cement-based concretes, The University of Alabama, Ann Arbor, 2021, p. 212.
[37] Y. Fang, J. Wang, X. Qian, L. Wang, P. Chen, P. Qiao, A renewable admixture to enhance the performance of cement mortars through a pre-hydration method, J. Clean. Prod. 332 (2022) 130095.
[38] Y. Fang, J. Wang, H. Ma, L. Wang, X. Qian, P. Qiao, Performance enhancement of silica fume blended mortars using bio-functionalized nano-silica, Constr. Build. Mater. 312 (2021) 125467.

[39] R.W. Balluffi, S.M. Allen, W.C. Carter, Kinetics of materials, John Wiley & Sons, 2005.
[40] J.W. Cahn, The kinetics of grain boundary nucleated reactions, Acta Metall. 4 (5) (1956) 449–459.
[41] J.J. Thomas, A new approach to modeling the nucleation and growth kinetics of tricalcium silicate hydration, J. Am. Ceram. Soc. 90 (10) (2007) 3282–3288.
[42] G.W. Scherer, J. Zhang, J.J. Thomas, Nucleation and growth models for hydration of cement, Cem. Concr. Res. 42 (7) (2012) 982–993.
[43] H.F. Taylor, Cement chemistry, Thomas Telford, London, 1997.
[44] S.C. Handbook, Atomic absorption spectrophotometry cookbook, Shimadzu Corporation. Kyoto, Japan, 2007.
[45] A. Cuesta, J.D. Zea-Garcia, D. Londono-Zuluaga, A.G. De la Torre, I. Santacruz, O. Vallcorba, M. Dapiaggi, S.G. Sanfélix, M.A.G. Aranda, Multiscale understanding of tricalcium silicate hydration reactions, Sci. Rep. 8 (1) (2018) 8544.
[46] K. Scrivener, R. Snellings, B. Lothenbach, A practical guide to microstructural analysis of cementitious materials, CRC Press Taylor & Francis Group, Boca Raton, 2016.
[47] D. Lin, B. Xing, Tannic acid adsorption and its role for stabilizing carbon nanotube suspensions, Environ. Sci. Tech. 42 (16) (2008) 5917–5923.
[48] A. Machner, M. Zajac, M.B. Haha, K.O. Kjellsen, M.R. Geiker, K. De Weerdt, Chloride-binding capacity of hydrotalcite in cement pastes containing dolomite and metakaolin, Cem. Concr. Res. 107 (2018) 163–181.
[49] M. Kamali, A. Ghahremaninezhad, Effect of Biomolecules on the Nanostructure and Nanomechanical Property of Calcium-Silicate-Hydrate, Sci. Rep. 8 (1) (2018) 1–16.
[50] I. Richardson, G. Groves, Models for the composition and structure of calcium silicate hydrate (C-S-H) gel in hardened tricalcium silicate pastes, Cem. Concr. Res. 22 (6) (1992) 1001–1010.
[51] Y. He, L. Lu, L.J. Struble, J.L. Rapp, P. Mondal, S. Hu, Effect of calcium–silicon ratio on microstructure and nanostructure of calcium silicate hydrate synthesized by reaction of fumed silica and calcium oxide at room temperature, Mater. Struct. 47 (1–2) (2014) 311–322.
[52] Y. Yan, S.-Y. Yang, G.D. Miron, I.E. Collings, E. L'Hôpital, J. Skibsted, F. Winnefeld, K. Scrivener, B. Lothenbach, Effect of alkali hydroxide on calcium silicate hydrate (C-S-H), Cem. Concr. Res. 151 (2022) 106636.
[53] H. Ma, Mercury intrusion porosimetry in concrete technology: tips in measurement, pore structure parameter acquisition and application, J. Porous Mater. 21 (2) (2014) 207–215.
[54] P. Mondal, Nanomechanical properties of cementitious materials, Northwestern University, 2008.
[55] W.C. Oliver, G.M. Pharr, An improved technique for determining hardness and elastic modulus using load and displacement sensing indentation experiments, J. Mater. Res. 7 (6) (1992) 1564–1583.
[56] R.-J.-M. Pellenq, A. Kushima, R. Shahsavari, K.J. Van Vliet, M.J. Buehler, S. Yip, F.-J. Ulm, A realistic molecular model of cement hydrates, Proc. Natl. Acad. Sci. 106 (38) (2009) 16102–16107.
[57] P.D. Tennis, H.M. Jennings, A model for two types of calcium silicate hydrate in the microstructure of Portland cement pastes, Cem. Concr. Res. 30 (6) (2000) 855–863.
[58] H.C. Pedrosa, O.M. Reales, V.D. Reis, M. das Dores Paiva, E.M.R. Fairbairn,, Hydration of Portland cement accelerated by CSH seeds at different temperatures, Cem. Concr. Res. 129 (2020) 105978.
[59] X. Kong, Z. Lu, Y. Zhang, Z. Zhang, Y. Jin, D. Wang, Effect of organic grinding aids on cement properties and the analysis via organic cement chemistry, J. Chin. Ceram. Soc. 40 (1) (2012) 49–55.
[60] E. Gartner, J. Young, D. Damidot, I. Jawed, Hydration of Portland cement, Structure and Performance of Cements 2 (2002) 57–113.
[61] P. Barnes, J. Bensted, Structure and performance of cements, CRC Press, 2002.
[62] J. Chen, L. Qiu, Q. Li, J. Ai, H. Liu, Q. Chen, Rapid hemostasis accompanied by antibacterial action of calcium crosslinking tannic acid-coated mesoporous silica/silver Janus nanoparticles, Mater. Sci. Eng. C 123 (2021) 111958.
[63] G. Han, S. Wen, H. Wang, Q. Feng, Interaction mechanism of tannic acid with pyrite surfaces and its response to flotation separation of chalcopyrite from pyrite in a low-alkaline medium, J. Mater. Res. Technol. 9 (3) (2020) 4421–4430.
[64] P. Chen, Y. Wang, S. He, P. Wang, Y. Xu, L. Zhang, Green synthesis of spherical calcium hydroxide nanoparticles in the presence of tannic acid, Adv. Mater. Sci. Eng. 2020 (2020).
[65] N. Dutta, S. Hazarika, T.K. Maji, Study on the role of tannic acid–calcium oxide adduct as a green heat stabilizer as well as reinforcing filler in the bio-based hybrid polyvinyl chloride–thermoplastic starch polymer composite, Polym. Eng. Sci. 61 (9) (2021) 2339–2348.
[66] J. Sherwood, Shape dependent iron oxide nanoparticles for simultaneous imaging and therapy, University of Alabama Libraries, 2018.
[67] Y. Zang, Q. Yang, P. Wang, X. Wang, D. Hou, T. Zhao, J. Chen, Molecular dynamics simulation of calcium silicate hydrate/tannic acid interfacial interactions at different temperatures: configuration, structure and dynamic, Constr. Build. Mater. 326 (2022) 126820.
[68] W.A. Tasong, C.J. Lynsdale, J.C. Cripps, Aggregate-cement paste interface: Part I. Influence of aggregate geochemistry, Cem. Concr. Res. 29 (7) (1999) 1019–1025.
[69] J. Grandet, J. Ollivier, Study of formation of calcium monohydrocarboaluminate by reaction of hydrated calcium with calcite aggregate in portland-cement paste, Cem. Concr. Res. 10 (6) (1980) 759–770.
[70] P. Yu, R.J. Kirkpatrick, B. Poe, P.F. McMillan, X. Cong, Structure of calcium silicate hydrate (C-S-H): Near-, Mid-, and Far-infrared spectroscopy, J. Am. Ceram. Soc. 82 (3) (1999) 742–748.
[71] J. Li, Q. Yu, H. Huang, S. Yin, Effects of Ca/Si ratio, aluminum and magnesium on the carbonation behavior of calcium silicate hydrate, Materials 12 (8) (2019) 1268.
[72] Y. Chiang, S.-W. Chang, Bridging the gap between NMR measured mean silicate chain length and nano-scale silicate polymorphism of calcium silicate hydrates, Cem. Concr. Res. 140 (2021) 106268.
[73] J. Li, W. Zhang, P.J. Monteiro, Structure and intrinsic mechanical properties of nanocrystalline calcium silicate hydrate, ACS Sustain. Chem. Eng. 8 (33) (2020) 12453–12461.